MOOSE Project Part III

Sadman Sakib

NE 533: Nuclear Fuel Performance

Submitted to:
Dr. Benjamin Beeler
Assistant Professor
Department of Nuclear Engineering
NC State University

Chapter 1

Introduction

In the rapidly evolving field of nuclear energy, the optimization of fuel rod design remains an important concern for enhancing efficiency and safety within Pressurized Water Reactors (PWRs). The MOOSE (Multiphysics Object-Oriented Simulation Environment) project designed for completion of 'NE 533: Nuclear Fuel Performance' is divided into three parts, each building upon the successes and data of the preceding segment, resulting in a comprehensive simulation of thermal and mechanical interactions within nuclear fuel elements. In the initial phase, the project addresses the fundamental thermal profiles of fuel pellets, setting the stage with both steady and transient heat load scenarios. The second part advances this by enhancing the thermal conductivity assumptions to refine the temperature distribution models. The final segment integrates these thermal calculations with tensor mechanics to simulate the stresses induced by thermal expansion and irradiation swelling, aiming to predict Pellet-Cladding Mechanical Interaction (PCMI) behaviors effectively.

In the first two parts, the dimensions of the fuel pin, including the fuel itself, the gap, and the cladding, are critically considered, alongside assumed values for thermal conductivity, to establish a realistic model. A specific focus is placed on the axial temperature distribution of the coolant, where coolant inlet temperature is 500 K, and the linear heat rate (LHR) at fuel centerline is 350 w/cm, aiming to uncover the axial location of peak centerline temperature. Part 3 asks to combine heat conduction and tensor mechanics in a fully thermo-mechanical simulation to get the stresses due to thermal expansion and irradiation induced swelling in the fuel. In part 2, thermal contact module was used to analyze the gap heat transfer. In part 3, thermo-mechanical contact has been used to look at PCMI beahviors. The boundary conditions has been reduced to a fuel surface temperature to eradicate complexities. Final analysis has been done considering both constant and axially varying linear heat rates (LHRs) to have a comparison between the results obtained from them.

To facilitate this analysis, the project assumes reasonable values for key parameters such as thermal conductivity, flow rates, and heat capacities, enabling a detailed simulation of temperature profiles at axial positions of 0.25 m, 0.5 m, and 1 m in part 2. In part 3, Young's modulus, Poisson's ratio, density and thermal expansion coefficient have been assumed to establish the thermo-mechanical simulation.

This report presents the findings from every parts of the MOOSE Project, incorporating insights gained from Part 1 and 2, and further refining the understanding through the choice of materials, mesh details, and the resolution of previously identified issues.

Chapter 2

Methodology

This section outlines the systematic approach adopted in this project to analyze the therm-mechanical behavior within a nuclear fuel pin. The study is designed to simulate temperature profiles across various axial positions within a fuel rod, then combining heat conduction and tensor mechanics in a fully thermo-mechanical simulation to get the stresses due to thermal expansion and irradiation induced swelling in the fuel rod, leveraging the capabilities of the MOOSE framework. The methodology encompasses the selection of materials, determination of thermal properties, equations which have been used, computational mesh design, and the implementation of boundary conditions reflective of operational conditions in PWRs.

2.1 Selection of Materials and their Properties

The fuel rod analyzed in this study consists of three primary components: the nuclear fuel, the gap, and the cladding. The dimensions specified for these components are a fuel radius of 0.5 cm, a gap thickness of 0.005 cm, and a cladding thickness of 0.1 cm, with the entire rod extending to a length of 1 cm (for part 1) and 1 m (for part 2). Table 2.1 shows all of the materials that have been used with their respective thermal properties.

Table 2.1: Selected materials and their thermal properties

Materials	Region	Heat Capacity $(J/g-K)$	Thermal Conductivity $(w/cm-K)$	Thermal Expansion Co-efficient (deg^{-1})
UO_2	Fuel	0.33	0.03	11×10^{-5}
Zr	Cladding	0.17	0.35	7×10^{-5}
He	Gap	-	0.0026	-

As tensor mechanics is included in part 3 to combine heat conduction and tensor mechanics in a fully thermo-mechanical simulation to get the stresses due to thermal expansion and irradiation-induced swelling in the fuel, some of the mechanical properties have been considered to calculate the desired properties. Table 2.2 shows all of the materials that have been used with their respective mechanical properties.

Table 2.2: Selected materials and their mechanical properties

Materials	Region	Density (g/cc)	Young's Modulus (psi)	Poisson's Ratio
UO_2	Fuel	10.98	180×10^5	0.35
Zr	Cladding	0.5	94×10^5	0.4

Before proceeding, the assumption made in some of the properties for the materials should be mentioned. Thermal expansion co-efficient and Young's Modulus for fuel and cladding have been underestimated by one order to accelerate the observation of swelling and PCMI. The accelerated observation helps to limit simulation time and amount of resource which was required by the simulation to run.

Here, thermal conductivity of UO_2 as a function of temperature has been considered which can be expressed as:

$$k_{temp} = \frac{1}{3.8 + 0.0217 \times T} \tag{2.1}$$

where, T is temperature and k_{temp} is thermal conductivity as a function of temperature.

2.2 Equations and other Parameters

We know, the heat conduction governing equation for axisymmetric cylindrical fuel rod can be expressed by equation 2.2:

$$\frac{1}{r}.\frac{\partial}{\partial r}\left(rk\frac{\partial T}{\partial r}\right) - q''' = \rho C_p \frac{\partial T}{\partial t} \tag{2.2}$$

Here, k is thermal conductivity of the fuel, r is radius of the fuel pin, ρ is the density of the fuel, C_p is the specific heat and q''' is volumetric heat generation.

Neutron flux varies axially, so does the linear heat rate (LHR). Let, a fuel rod which has a length of $2Z_0$, so the midpoint is Z_0. Then, the equation for axial LHR can be expressed by equation 2.3:

$$LHR\ (\frac{z}{Z_0}) = LHR^{\circ}\ cos\ [\ \frac{\pi}{2\gamma}\ (\frac{z}{Z_0 - 1})\ ] \tag{2.3}$$

Here, LHR° is the midpoint linear heat rate. A typical value for γ is 1.3 which reduces $\frac{\pi}{2\gamma}$ to 1.2.

Coolant temperature varies axially as well which can be expressed by equation 2.4:

$$T_{cool} - T_{cool}^{in} = \frac{1}{1.2}\frac{Z^{\circ} \times LHR^{\circ}}{\dot{m}C_{pw}}\left\{sin(1.2) + sin\left[1.2\left(\frac{z}{Z^{\circ} - 1}\right)\right]\right\} \tag{2.4}$$

Here, T_{cool} is coolant temperature varying axially, T_{cool}^{in} is the coolant inlet temperature, $\dot{m}$ is mass flow rate and C_{pw} is specific heat capacity of coolant which is water.

The change in the volume of the fuel rod due to swelling (due to solid and gaseous fission products, combined swelling effect) can be expressed by equation 2.5:

$$\epsilon_{swelling} = 5.577 \times 10^{-2}\rho\beta + 1.96 \times 10^{-28}\rho\beta(2800 - T)^{11.73}e^{-0.0162(2800-T)}e^{-17.8\rho\beta} \quad (2.5)$$

Here, β is the burnup in %FIMA (fissions per initial metal atom).

Table 2.3 refers to the parameters used in equations 2.3 and 2.4. The density values for fuel and cladding used in equation 2.5 are given in table 2.2.

Table 2.3: Given/Assumed Parameters

Parameter	Given/Assumed	Value	Unit
Linear heat rate, LHR	Given	350	w/cm
Coolant inlet temperature, T^{in}_{cool}	Given	500	K
Coolant flow rate, $\dot{m}$	Assumed	0.24	kg/s
Specific heat capacity of ccolant, C_{pw}	Assumed	4200	$J/kg - K$

2.3 Mesh Design

A structured mesh was carefully designed to capture the complexities of the fuel rod geometry, ensuring sufficient resolution in areas of interest. Mesh sensitivity analysis was conducted to ascertain the impact of mesh density on simulation accuracy. The detailed information on mesh convergence analysis will be included at the results and discussion section.

For part 2, side sets between the fuel and cladding subdomains were set up to delete the gap region which was included in the previous segment. Then, a thermal contact block was set up to include the gap heat transfer. Here, gap thermal conductivity was assumed as 0.0026 $w/cm - K$. For part 3, as PCMI was intended to be analyzed, geometry was re-arranged to set fuel and cladding parts separately and merge them together by keeping a gap of 0.005 cm.

Chapter 3

Results & Discussion

As first part of the project, temperature profiles for steady state and transient conditions were simulated. Primary assumptions were:

- Heat was only generated in the fuel.
- In steady state, the heat generation is constant.
- All material properties (in case of constant thermal conductivity) and all material properties except thermal conductivity (in case of temperature dependent thermal conductivity) were unchanged over time and temperatures.
- There is good thermal contact between each block.

Table 3.1: Temperature profiles for steady state condition (considering constant and temperature dependent thermal conductivity)

Point	Analytical Result (K)	Simulated Results ($k_{constant}$) (K)	Deviation (%)	Simulated Results (k_{temp}) (K)
Fuel Centerline	1758.18	1768.16	0.568	1682.96
Fuel Surface	829.78	811.345	2.22	815.02
Cladding Inner Surface	615.53	609.941	0.91	609

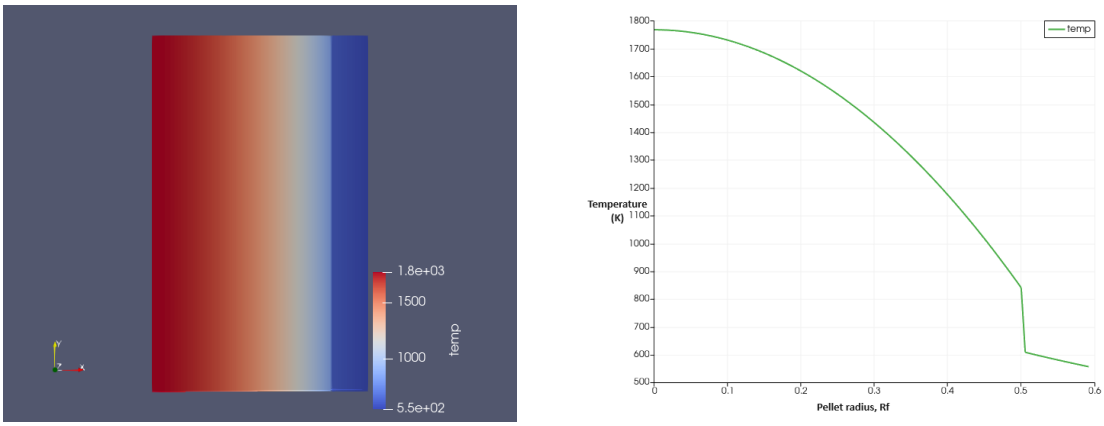

(a) (b)

Fig. 3.1: Colored contour plotting of the geometry (a) and temperature vs pellet radius plotting (b) of the steady state condition considering constant thermal conductivity

The results are presented in table 3.1 and figure 3.1. There was a sudden increase in centerline temperature which was observed while analyzing the simulation

of transient condition; initial temperature ($550K$) was less than the steady state temperature ($960K$). Maximum centerline temperature was $1242.33K$ which is far below the UO_2 melting temperature ($3138K$). At $61.75s$, the system reaches a steady state temperature ($\approx 960K$). The steady state had been reached at around $61.75s$ and then it was extended to $84.25s$ to display the steady state region of the curve.

One of the issues that was in the first part of the project was 'use of a very refined mesh'. Mesh convergence analysis was not done in the previous segment of the project and it has been addressed in the second part. The process of mesh convergence involves decreasing the element size and analysing the impact of this process on the accuracy of the solution. Typically, the smaller the mesh size, the more accurate the solution as the behavior of the design or product is better sampled across its physical domain. Table 3.2 shows the results obtained at various mesh sizes. The result obtained analytically ($1758.18K$) has been stated as the standard value and considering the deviation, $nx \times ny = 200 \times 300$ has been considered for the analysis.

Table 3.2: Analysis of Mesh Convergence

$nx \times ny$	Axial location for peak temperature (cm)	Temperature (K)
150×7	57	1507.23
150×200	51	1510.4
200×300	51	1659.87
200×500	51	1659.87
1000×1000	51	1616.52

Fig. 3.3 shows temperature profiles at different axial positions. The results express the trend of temperature rising from $z = 0$ to fuel centerline and then falling to a lower level at $z = 1$ which is expected. In all graphs, the presence of the sharp drop-off in the temperature profile near the edge of the fuel suggests a consistent thermal boundary where the heat is being transferred from the fuel to the coolant, cladding or other mediums.

Fig. 3.2 depicts the axial position for peak fuel centerline temperature. It has been found at $z = 0.51$. Ideally, it should have been around $z = 0.6$. The deviation from the ideal result can be due to many reasons. Flow rate can be adjusted to simulate a more ideal result. Nonetheless, the temperature profile, if compared with the profile obtained from part I, seems reasonable. The peak centerline temperature was around $1758K$ in part I and the result of part II agrees well with it.

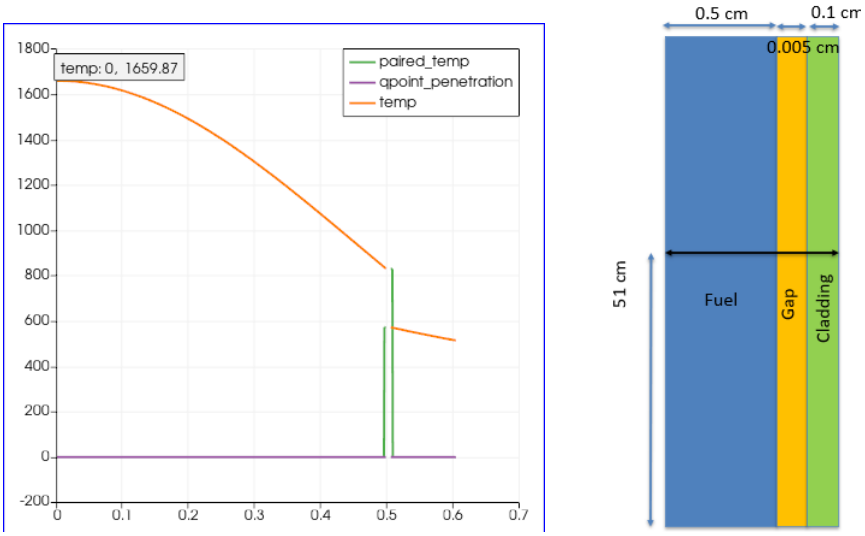

(a) Temperature profile at $z = 0.51$

(b) Schematic diagram of the fuel pin

Fig. 3.2: Axial location of peak fuel centerline temperature

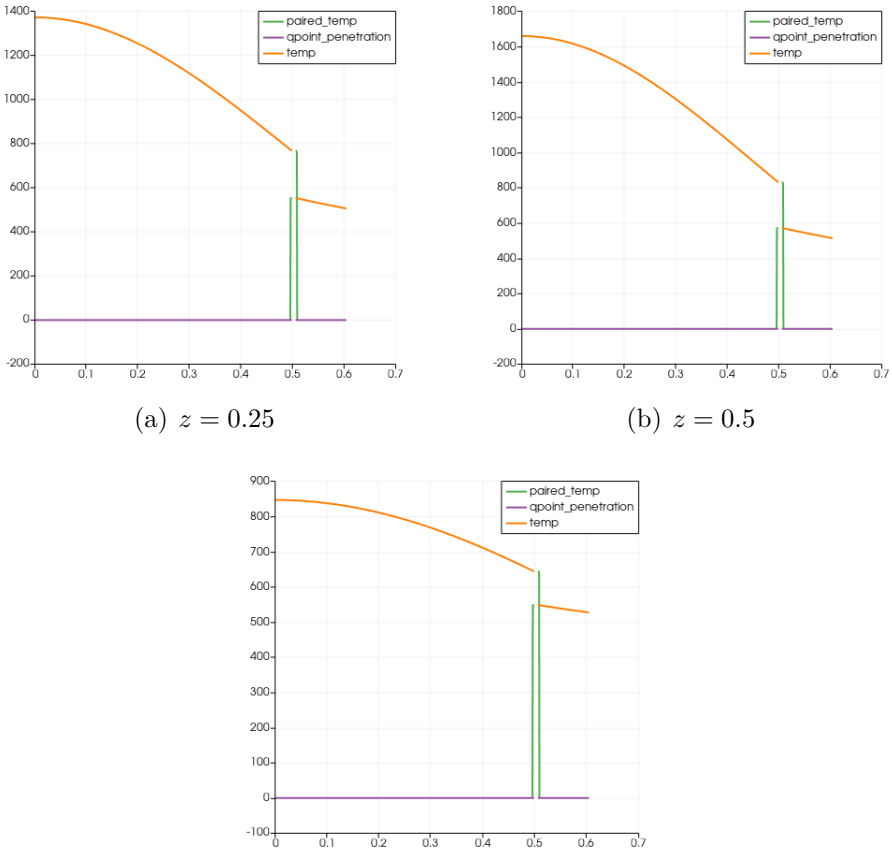

(a) $z = 0.25$

(b) $z = 0.5$

(c) $z = 1$

Fig. 3.3: Temperature profiles at different axial positions

The final part of the project combines heat conduction and tensor mechanics in a fully thermo-mechanical simulation to get the stresses due to thermal expansion and irradiation-induced swelling in the fuel. 3 kinds of stresses have been analyzed: normal stress acting on the X face in the X direction (σ_{XX}), normal stress acting on the Y face in the Y direction (σ_{YY}) and von-mises stress.

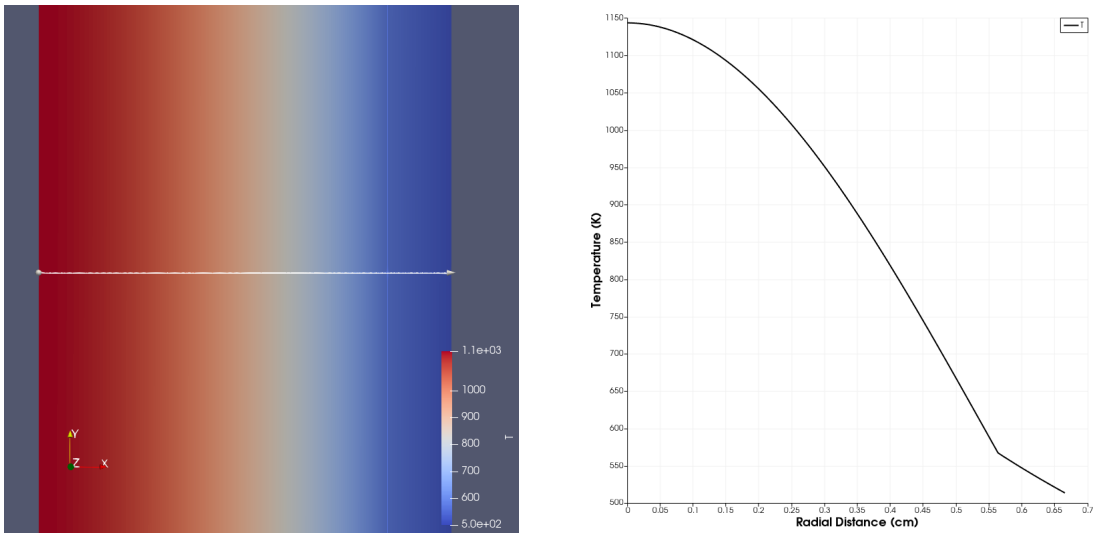

(a) (b)

Fig. 3.4: Radial temperature profile of the fuel rod (a) & temperature vs radial distance plotting (b)

Temperature profile over radial direction, from (0, 50) to (0.66552, 50) has been portrayed by figure 3.4. The trend of the temperature profile abides by the temperature profiles which have been observed in part 1 and 2.

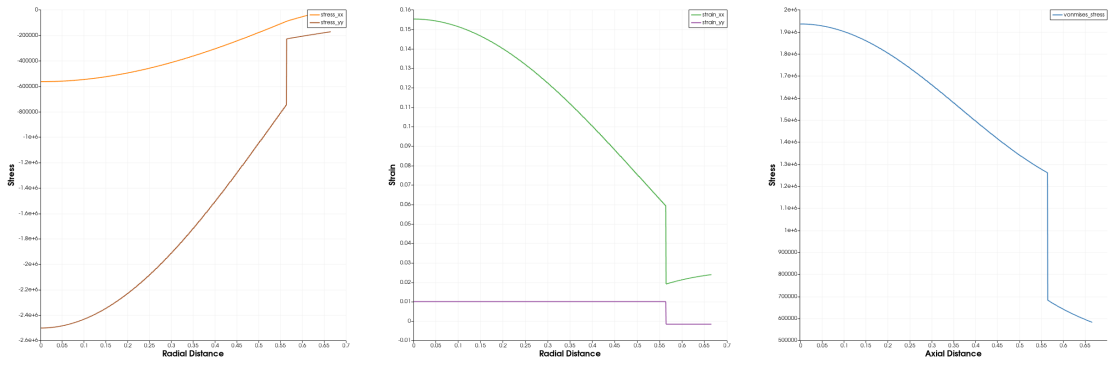

(a) (b) (c)

Fig. 3.5: Stress profiles in the radial direction. (σ_{XX}) (a), (σ_{YY}) (b) and von-mises stress (c) vs radial distance

Figure 3.5 depicts stress profiles in the same radial direction that has been considered earlier. Normal stress acting on the X face in the X direction increases

from fuel to cladding, showing inverse relation with the temperature. But other two stresses kept on increasing with radial direction from left to right, showing same trend as of the temperature.

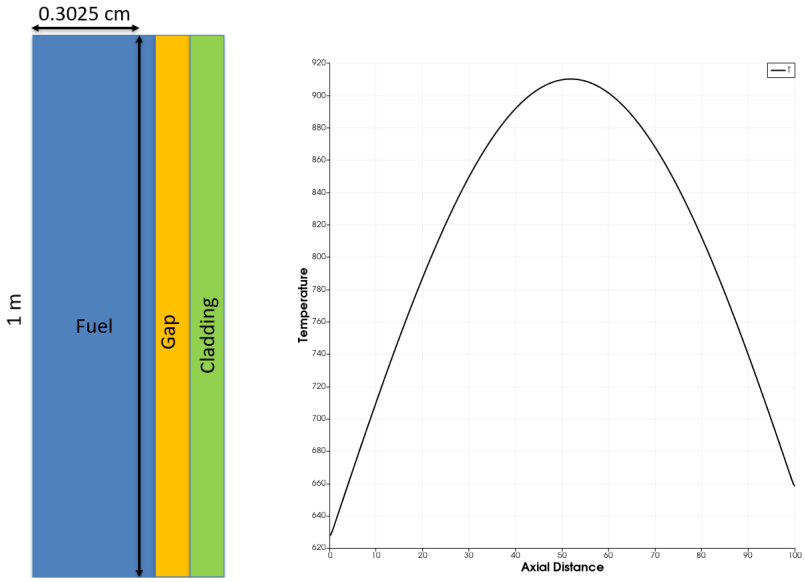

(a) (b)

Fig. 3.6: Schematic diagram of the fuel rod, black arrow portraying the axial direction being studied (a) & temperature vs axial distance plotting (b)

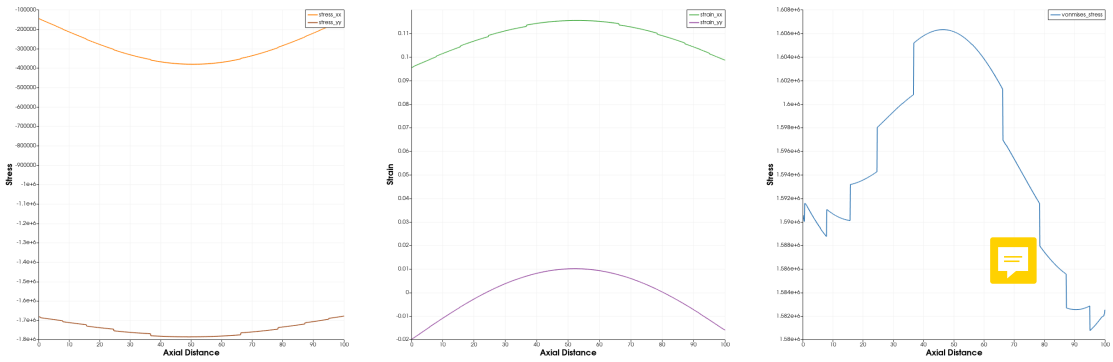

(a) (b) (c)

Fig. 3.7: Stress profiles in the axial direction. (σ_{XX}) (a), (σ_{YY}) (b) and von-mises stress (c) vs axial distance

Figure 3.7 depicts stress profiles in the same axial direction that has been considered earlier. Normal stress acting on the X face in the X direction shows inverse relation with the temperature which has been observed in 3.6. But other two stresses portrayed similar relation with the temperature. These trends are on par with the observations collection from the study of radial direction.

Chapter 4

Conclusion

Through the simulation of temperature profiles at axial positions $z = 0.25, z = 0.5$ and $z = 1$, a mapping of thermal behavior axially throughout the fuel has been established. With a coolant inlet temperature (T^{in}_{cool}) set at 500 K and a linear heat rate at fuel centerline, LHR° of 350 W/cm, the simulations have pinpointed the axial location of peak centerline temperature, thereby identifying potential hot spots and regions of thermal significance.

The temperature profiles across the different axial positions have remained consistent with the anticipated distribution of heat within a fuel rod. The peak temperature at almost the mid-length (z=0.51) suggests a higher thermal load in this region, aligning with the core's expected power peaking factors. This central hot spot necessitates further attention to ensure the integrity of the fuel rod over its operational life.

The final part of the project combined heat conduction and tensor mechanics in a fully thermo-mechanical simulation to get the stresses due to thermal expansion and irradiation-induced swelling in the fuel. Pellet-cladding mechanical interaction (PCMI) with significant swelling can be observed at t = 2s and t = 2.25s of the simulation. Here, the time required for the PCMI does not reflect the real-life scenario. But each time step can be assumed as a longer time of fuel operation. Thermal expansion co-efficient and Young's Modulus for fuel and cladding have been underestimated by one order to accelerate the observation of swelling and PCMI. The accelerated observation helps to limit simulation time and amount of resource which was required by the simulation to run.

Through the seamless integration of three critical phases—thermal modeling, thermal conductivity enhancement, and the combination of these models with mechanical stress simulations—the project demonstrated the powerful capability of MOOSE in addressing complex engineering challenges surrounding a nuclear reactor fuel. The insights gained from theese 3 parts of MOOSE project extend beyond the immediate applications in nuclear technology, providing a framework that can be adapted to solve other complex multi-physical problems in future generation advanced nuclear reactors.